AIAA JOURNAL
Vol. 40, No. 12, December 2002

Spectrally Filtered Raman/Thomson Scattering Using a Rubidium Vapor Filter

Wonchul Lee* and Walter R. Lempert†
The Ohio State University, Columbus, Ohio 43210

A new spectrally filtered light scattering apparatus is presented based on a diode laser injected seeded titanium: sapphire laser and rubidium vapor filter at 780.24 nm. It is shown that the realizable line center attenuation of quasi elastically scattered light, limited by a residual broad spectral linewidth, unseeded, component to the laser output, is as high as 1.67×10^5 using the laser system alone. Preliminary measurements indicate that incorporation of a set of dispersing prisms and a stimulated Brillouin scattering phase conjugate mirror external to the laser provides an additional approximate factor of 10 extinction. The utility of the system for measurement of electron density and temperature by Thomson scattering is demonstrated in a 3950-Pa (30-torr) argon dc discharge. At 100-mA current, an electron density of 3.7×10^{13} cm^{-3} is measured on the discharge centerline with a 2σ value of statistical uncertainty equal to 8.0×10^{11} cm^{-3}. The corresponding electron temperature is 0.63 ± 0.025 eV.

Introduction

THOMSON scattering is a well-known technique for determination of spatially resolved electron density and electron temperature (see Ref. 1). Similar to molecular Rayleigh scattering, Thomson scattering refers to the quasi-elastic scattering of optical radiation by free electrons in a plasma. Whereas the cross section for free electron scattering is approximately 100 times greater than that for Rayleigh scattering of common diatomic molecules, such as nitrogen, the typically low free electron number density in weakly ionized plasmas ($\sim 10^{10}$–10^{13} cm^{-3}) results in relatively low scattering signal. Detection of such inherently weak signal is aggravated by the desired scattering being superimposed upon what is often a much more intense interference due to elastic scattering from window and wall surfaces and/or, in the case of molecular plasmas, Rayleigh scattering from the heavy species. For high electron temperatures, of order tens of electron volts[2] (or greater[3]), the corresponding spectral broadening is sufficient that ordinary grating spectrometers can be used to discriminate the wings of the quasi-elastic Thomson scattering from the much more intense, spectrally narrow Rayleigh and/or elastic scattering. The problem is particularly acute, however, for plasmas with electron temperature of order 1 eV (or less). Noguchi et al.[4] have recently presented Thomson scattering measurements in an approximately 1-eV microdischarge plasma using a new instrument that featured a triple-grating spectrometer, incorporating a physical blocking mask in the focal plane between the first and second grating. This mask acted as an "inverse" slit, blocking light in a 1-nm bandwidth centered on the laser excitation frequency, while passing more spectrally broadened scattering. Using this instrument, they were able to make measurements within 0.30 mm of the microdischarge wall, reporting electron densities in the range 0.6×10^{13} to 1.0×10^{13} cm^{-3} and electron temperatures in the range 0.4–1.6 eV.

As an alternative approach to a physical mask, several optical diagnostic techniques based on the use of atomic/molecular vapor filters as narrow bandwidth "notch" filters and/or as spectral discriminators have recently been developed. The basic idea, common to all such techniques, it to utilize a narrow spectral linewidth laser excitation source that is tuned to a strong absorption resonance of an atomic or molecular vapor. A vapor cell is then inserted in the path between the scattering volume and the detector. This provides an efficient means by which elastic scattering interferences can be highly attenuated (by as much as $\sim 10^5$), whereas slightly spectrally shifted scattering (by as little as approximately 0.10 nm) can be highly transmitted. The use of such vapor filters for Raman scattering dates to near the discovery of the Raman effect itself (see Ref. 5). More recently, continuous wave (cw) Raman instruments incorporating mercury vapor[6] and rubidium vapor[7,8] have been reported. With the advent of high-intensity, pulsed laser sources as common laboratory tools, a variety of new vapor filter-based techniques for application to remote sensing,[9] flowfield imaging,[10] and combustion[11,12] have been developed.

In this paper we present new results obtained using a rubidium vapor filter in combination with a diode laser injection seeded, narrow spectral bandwidth titanium:sapphire laser at 780.24 nm. Rubidium vapor is attractive because it has an exceedingly strong absorption band in the near infrared (IR), a wavelength region in which excellent laser sources and detectors are available. It also has relatively high vapor pressure and relatively low chemical reactivity so that filter construction is straightforward. The primary goal of this work is to demonstrate the utility of the new system for low wave number inelastic scattering diagnostics, such as pure rotational Raman and Thomson scattering, in weakly ionized molecular plasmas. The laser system, based on that developed by Rines and Moulton,[13] and essentially identical to that previously used for filtered scattering diagnostics by Finkelstein et al.[14] and Zaidi et al.,[15] consists of the following basic components. The second harmonic output of a commercial Q-switched Nd:YAG laser is used as a pump source for a bread board titanium:sapphire laser, which is injection seeded using a single-frequency external cavity diode laser. The principal differences between this laser system and that reported by Finkelstein et al.[14] is the use of the diode laser seed source, which substitutes for an argon-ion pumped cw titanium:sapphire ring laser, and the use of injection seeding, as opposed to injection locking. This results in a significant decrease in cost and complexity, but has some disadvantages, which will be discussed in subsequent sections. The system is also conceptually similar to that recently described by Bakker et al.[16] who obtained Thomson scattering spectra in a glow discharge by combination of a grazing incidence dye laser with a sodium vapor filter. This system has the advantage that the laser is readily available commercially and is relatively simple. The filter, however, is somewhat more complex.

Experimental

Figure 1 shows a schematic diagram of the filtered scattering apparatus. The titanium:sapphire laser cavity is essentially identical to that described in Ref. 13 but is pumped by the second harmonic output of a commercial (Continuum Powerlite Precision 8000) 10-Hz repetition rate Q-switched Nd:YAG laser. The pump laser output of

Received 6 March 2002; revision received 1 August 2002; accepted for publication 9 August 2002. Copyright © 2002 by the American Institute of Aeronautics and Astronautics, Inc. All rights reserved. Copies of this paper may be made for personal or internal use, on condition that the copier pay the $10.00 per-copy fee to the Copyright Clearance Center, Inc., 222 Rosewood Drive, Danvers, MA 01923; include the code 0001-1452/02 $10.00 in correspondence with the CCC.

*Graduate Student, Department of Chemistry.
†Associate Professor, Departments of Mechanical Engineering and Chemistry. Associate Fellow AIAA.

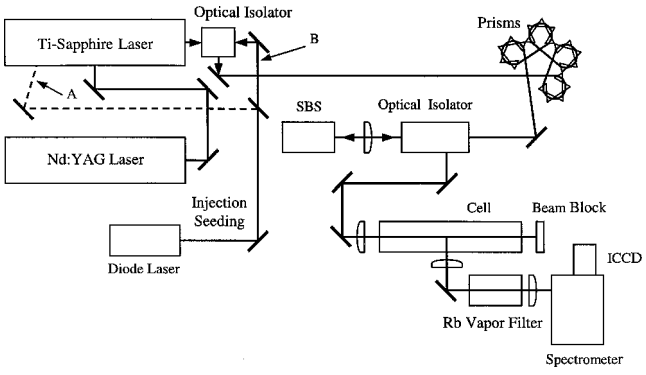

Fig. 1 Schematic diagram of filtered Thomson scattering apparatus; to rotate the scattering image parallel to the spectrometer input slit, a pair of mirrors is actually inserted between the cell and detector.

approximately 260 mJ/pulse is split into four parts, each of which pumps a single surface of one of two titanium:sapphire crystals. Each crystal surface is located in the intermediate field of a 130-cm focal length plano-convex lens (~60 cm before the waist), which partially focuses the ~8-mm-diam pump beam to a cross section of ~2–3 mm at the crystal surface. An external cavity diode laser (Newport Model 2010) is used for injection seeding, which has been performed in two configurations, labeled A and B in Fig. 1. Configuration A, similar to that described in Ref. 14, injects the seed laser using the very small (~3%) reflection of horizontally polarized light at near Brewster's angle from a quartz flat inserted into the cavity. This has the advantage of simplicity, but poor coupling efficiency. Configuration B couples the seed laser through the cavity output coupler using a Faraday rotation optical isolator. In some experiments, the output of the injection seeded laser is externally dispersed using a "prism monochromator" identical to that described by Bakker et al.,[16] followed by a stimulated Brillouin scattering (SBS) phase conjugate cell (see Ref. 17). As will be described in the next section, the purpose of this is to minimize interference from a small residual broadband, "nonseeded" component of the laser output. Ignoring this broadband component, the laser output energy is approximately 60 mJ/pulse, with spectral bandwidth of ~150 MHz (corresponding to one or two longitudinal modes). The individual pulse duration is ~30 ns.

Scattering is 1:1 imaged at 90 deg using a pair of mirrors and $f/4$ lenses to rotate the image of the Raman/Thomson scattering parallel to the entrance slit of an optical multichannel analyzer (OMA) system, consisting of a 0.25-m spectrometer and a GEN IV near-IR microchannel plate intensified charge-coupled device (ICCD) camera. Loose focusing of the titanium:sapphire laser (with a 40-cm focal length plano-convex lens) results in a cylindrical sampling volume 20–50 μm (defined by slit) in diameter by 5 mm in length. According to manufacturer's specifications (which have not been verified), the ICCD has a quantum efficiency of order 25–30% at 780 nm, which greatly facilitates the scattering diagnostics. The spectrometer is operated with an input slit of between 20 and 50 μm. A 5-cm path length rubidium vapor cell, heated to a temperature of 320°C, is placed in the detection path, between the scattering cell and the OMA. The vapor cell is quite simple, consisting of a single piece of 25.4-mm-diam quartz tubing containing the rubidium, with optical flats fused to each end. The cell is heated by wrapping with standard laboratory heating tape and is temperature controlled to ±1 K using a thermocouple (placed on the outside of the cell) and a simple feedback controller. To minimize condensation of rubidium vapor on the cell windows, a pair of evacuated 25.4-mm-diam quartz extension tubes are fused to the ends of the cell. Heating of these tubes minimizes the temperature gradient at the cell windows and, therefore, rubidium vapor condensation. Some window degradation, presumably due to chemical reaction, is also observed. After approximately 200 h of operation at high temperature, the cell transmission was measured to have dropped from approximately 0.85 (due to Fresnel losses) to approximately 0.50.

Rotational Raman spectra were obtained in a static cell, essentially identical to that used previously for Q-branch Raman spectra.[18] Thomson scattering spectra were obtained in a similar cell to which a pair of electrodes had been added. The electrodes were 6.35-mm-diam stainless-steel rods, positioned in the center of the cell, separated by a spacing of 25.4 mm. All spectra were integrated on the ICCD sensor for a period of between 1 and 10 min.

Results and Discussion

Characterization of System Extinction Without SBS Cell

Figure 2 shows a Fourier transform transmission spectrum of the rubidium vapor cell at 320°C, along with a least-squares fit to a simple spectral model of the $5s^2S_{1/2} - 5p^2P_{3/2}$ transition at 780.24 nm. The spectrum was measured with a commercial (Bruker IFS-66) Fourier transform spectrometer, operated with a spectral resolution of 0.25 cm^{-1}, a tungsten lamp source, and a silicon photodiode detector. As can be seen Fig. 3, which is a calculation of the absorbance, the 780.24-nm transition is made up of 12 individual components, which result from a combination of hyperfine splitting and natural isotopic abundances.[19,20] Whereas the theoretical absorption of the cell is exceedingly high, with calculated peak absorbance of $\sim 3 \times 10^6$, the realizable attenuation of elastic and/or Rayleigh/Mie scattering is limited, as reported previously,[15,21,22] by the existence of a small, but significant, broad spectral bandwidth (~1 nm) component to the narrow linewidth titanium:sapphire laser output. Note that this component is not believed to be due to amplified spontaneous emission (ASE). Rather, it is believed to result from an unlocked component of the output intensity, the magnitude of which, as will be shown, depends on the injected seed laser power. This view is supported by the observation that insertion of a card directly in front of the high reflector in the rear of the titanium:sapphire cavity completely eliminates the broadband component, that is, it requires "lasing" feedback. To evaluate the realizable extinction of Rayleigh/Mie scattering, a detailed set of measurements have been performed using injection seeding configurations A and B in Fig. 1, both with and without incorporation of the dispersing prisms and SBS cell.

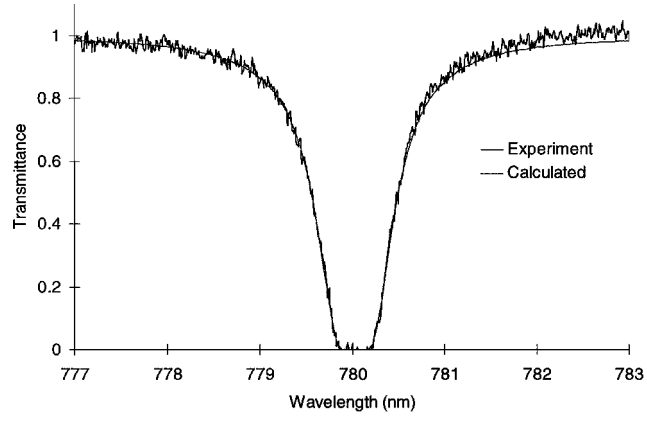

Fig. 2 Experimental transmission of 5-cm path length rubidium vapor cell at 320°C and least-squares fit to spectral model.

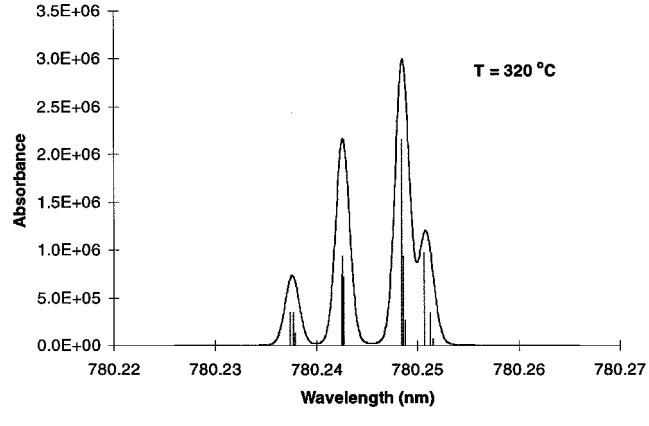

Fig. 3 Modeled absorbance of rubidium vapor cell including position and relative contribution of 12 hyperfine/isotope components.

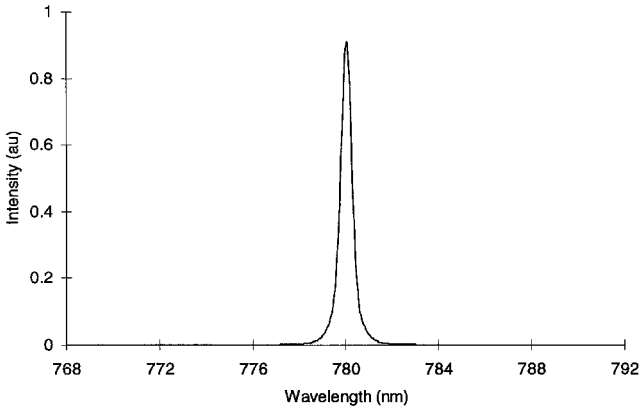

Fig. 4a Scattering spectrum of static cell of 500 torr of N_2 at room temperature; no vapor filter employed.

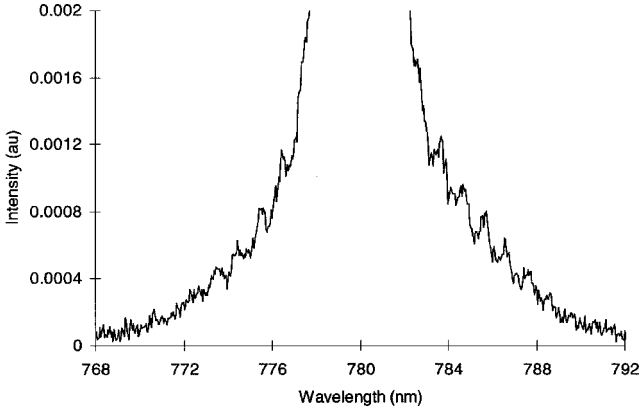

Fig. 4b Spectrum in Fig. 4a, 500× blowup; intensity axis normalized to peak intensity in Fig. 4a.

As a baseline for comparison, Fig. 4a is a scattering spectrum from a static cell of 500 torr of nitrogen at room temperature, obtained without either injection seeding of the laser or insertion of the rubidium vapor filter into the detection path. It appears to be a single central component with linewidth of 0.56-nm full width at half maximum (FWHM) representing a convolution of the unseeded laser linewidth with the ~0.20-nm spectral resolution of the spectrometer. Figure 4b is a 500× blowup of the spectrum in Fig. 4a in which the intensity axis is normalized to the peak of the quasi-elastic Rayleigh/Mie scattering signal from Fig. 4a. It can be seen that the peak intensity of this central quasi-elastic scattering signal is a factor of ~5000 greater than that for the individual rotational Raman transitions. (Note that a portion of the central scattering component is almost certainly due to stray elastic scattering from windows and surfaces.) Moreover, note that at our targeted conditions of $\sim 10^{13}$-cm^{-3} electron density, the peak quasi-elastic Thomson scattering signal will be a factor of approximately 20 times lower than the peak Raman signal observed in Fig. 4b.

Figure 5 illustrates the attenuation of quasi-elastic scattering that was achieved using injection seeding alone. (Results obtained incorporating the SBS cell are presented subsequently.) Figures 5a and 5b show the results of seeding configuration A, in which the circulating seed power within the titanium:sapphire cavity was measured to be ~50–100 μW (1–2% of the seed laser power). Figures 5a and 5b are identical to Figs. 4a and 4b, except that injection seeding of the laser has resulted in a considerably narrowed spectral linewidth, with apparent FWHM, limited by the spectrometer resolution, of ~0.20 nm. In this case, it can be seen that the peak intensity of the central quasi-elastic scattering signal is a factor of ~2000 greater than the peak rotational Raman signal. Figure 5c is another identical, similarly normalized spectrum, except that it was obtained using the rubidium filter. Comparison of Figs. 5a and 5c shows that the line center relative intensity of the central scattering component is reduced by a factor of ~3000 when the rubidium filter is employed. In addition, it can be seen from Fig. 5c that the residual transmitted

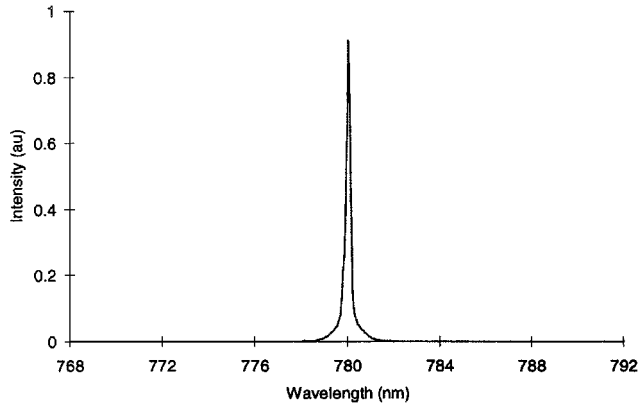

Fig. 5a Scattering spectrum of static cell of 500 torr of N_2 at room temperature employing injection seeding configuration A; no vapor filter employed.

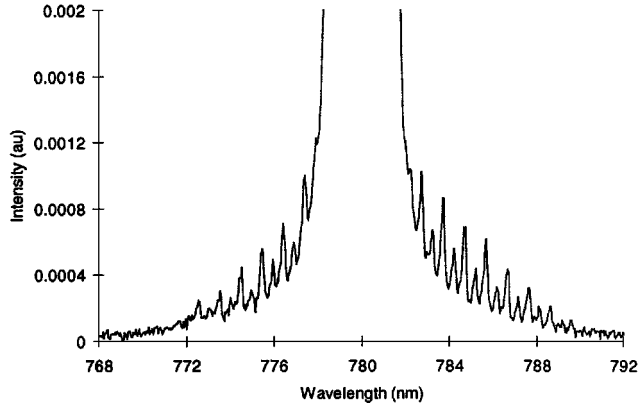

Fig. 5b Spectrum in Fig. 5a, 500× blowup; intensity axis normalized to peak intensity in Fig. 5a.

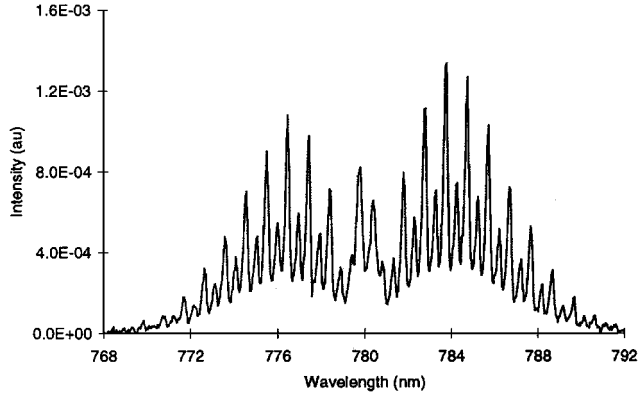

Fig. 5c Pure rotational Raman spectrum of 500 torr of N_2 at room temperature employing seeding configuration A without SBS cell; intensity axis normalized to peak intensity obtained without incorporation of vapor filter.

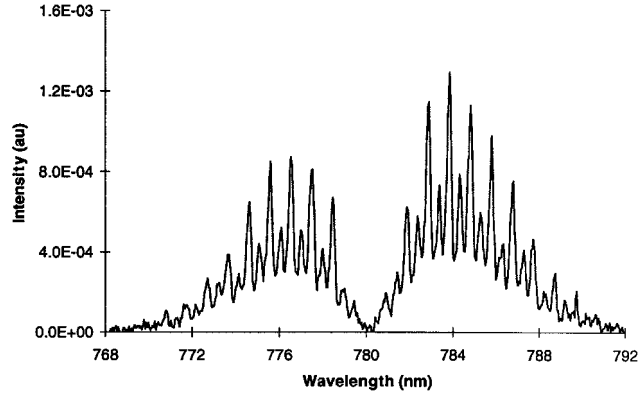

Fig. 5d Identical to Fig. 5c except seeding configuration B employed.

central component has a "hole" in the center, corresponding to the narrow linewidth absorption cell. Note that the spectra shown in Figs. 5b and 5c were obtained with a laser pulse energy incident to the scattering cell of ~50 mJ/pulse. The intensity was integrated on the ICCD detector for 1 min.

Figure 5d shows the rotational Raman spectrum obtained employing seeding configuration B. In this case, the circulating seed power in the titanium:sapphire cavity is increased to ~1 mW, although the laser output is reduced by ~30% due to transmission losses in the optical isolator. It can be seen that the relative intensity of the central scattering component has been very greatly reduced, to the extent that it is difficult to determine from inspection. In fact, the peak residual fractional intensity, measured as described and shown in a subsequent section, is $\sim 6 \times 10^{-6}$ so that the peak rotational Raman intensity is now ~200 times greater than the peak residual, transmitted central component scattering. Whereas Thomson scattering is the primary motivation for the development of this instrument, it is clear that the system provides significant capability for pulsed rotational Raman spectroscopy. For the 1-min integration period employed to obtain the spectra in Fig. 5, the resulting signal-to-noise ratio is approximately 50, corresponding to a measurement limit of approximately 1300 Pa (10 torr). It is anticipated, though has not been demonstrated, that, based on the read noise of the CCD array, this sensitivity limit could be decreased by at least one additional order of magnitude by increasing the integration time.

The spectra in Fig. 5 illustrate the well-known fact that the laser spectral purity P, defined as the ratio of the narrowband component of the injection seeded laser pulse to the total output, is a strong function of the circulating seed pulse energy. The injection seeding process is described in detail by Barnes et al.,[22,23] who show that the circulating seed energy required to achieve a given spectral purity scales as

$$E_{\text{seed}} \propto P/1 - P \tag{1}$$

when other factors, such as the spatial and spectral overlap between the seed laser beam and the titanium:sapphire cavity modes, are constant. Clearly, in the limit when P approaches one, the required seed energy increases rapidly. By the preceding definition, the spectral purity that we have achieved employing seed configuration B is on the order of 0.9998. [Note that we arrive at this number by 1) the assumption that the effective spectral linewidth of the residual transmitted light, which includes the spectrometer instrument function, is a factor of ~10 greater than that for the seeded light and 2) that approximately 75% of the broadband component is absorbed by the filter.] Although we have not performed an exhaustive literature search, this represents, to our knowledge, an improvement of approximately a factor of 10 over that reported in Ref. 21 for the third harmonic and Ref. 23 for the fundamental, using cw injection seeding. Because of limits in the seed power of our external cavity laser system, it is not clear whether (or how close to) a practical limit we have achieved.

Thomson Scattering Spectra

Figure 6 shows a filtered Thomson scattering spectrum obtained from a dc argon "constricted" glow discharge also obtained without incorporation of the dispersing prisms and SBS cell. The argon pressure is 3950 Pa (30 torr) and the discharge current is 100 mA. The constricted glow is ~1–2 mm in diameter and is stabilized by incorporation of a 500-Ω current limiting ballast resistor in series with the dc discharge. Approximately 25% of the total applied 20 W is dissipated across the resistor. Although this is somewhat inefficient, it provides a simple means to create a reasonably stable discharge with relatively high ($\sim 10^{13}$ cm^{-3}) electron density. Figure 6a shows the exceedingly weak Thomson scattering signal superimposed upon the relatively large argon spontaneous emission. Despite employing a gated ICCD camera, it can be seen that the spontaneous emission is many orders of magnitude more intense than the Thomson signal. This is confirmed in Fig. 6b, which is a 200× blowup of the spectrum in Fig. 6a.

Figure 7 is a least-squares fit of the experimental spectrum in Fig. 6b to a simple incoherent Thomson scattering model.[1] The

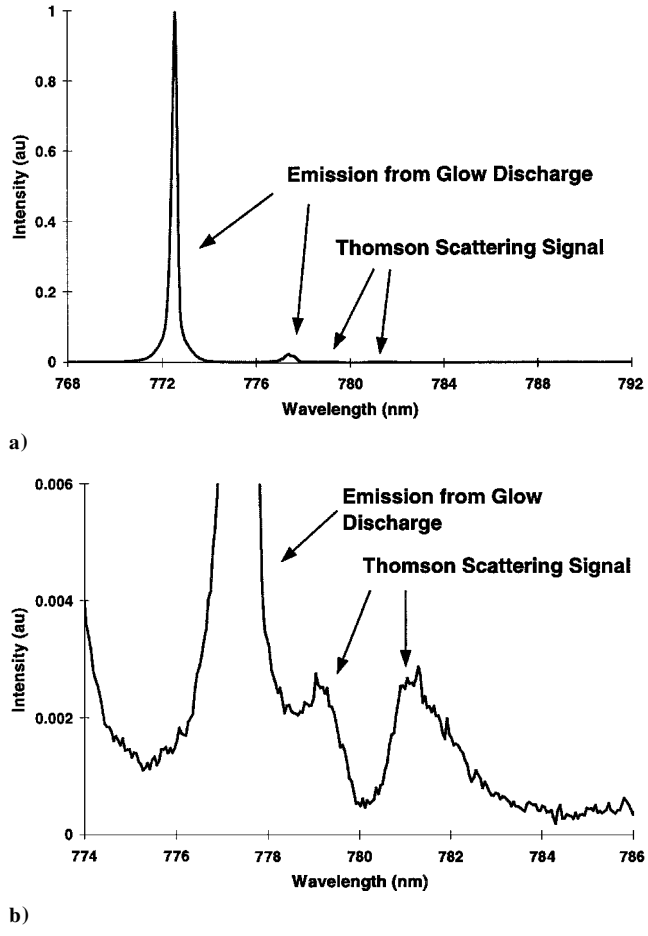

Fig. 6 Thomson scattering spectrum obtained using seeding configuration B from argon constricted glow dc discharge; argon pressure 3950 Pa and discharge current 100 mA. Dispersing prisms and SBS cell not employed.

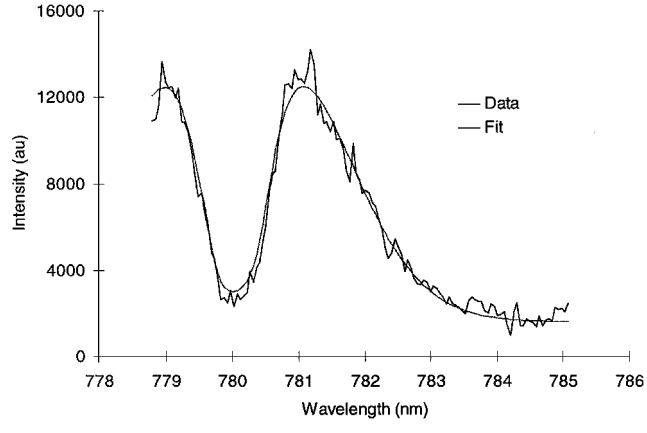

Fig. 7 Least-squares fit to Thomson spectrum of Fig. 6b; electron density 3.7×10^{13} cm^{-3} and electron temperature 0.63 eV.

model assumes a Gaussian scattering spectrum, with half width at half maximum γ given by

$$\gamma = (2\lambda_{780}/c)\sqrt{2\ln(2)kT_e/m_e}\,\sin(\theta/2) = 2.57\sqrt{T_e}\,\sin(\theta/2) \tag{2}$$

where T_e is the electron temperature in electron volts, θ is the scattering angle, and γ is in nanometers. The model incorporates the measured transmission profile of the rubidium filter (Fig. 2), convolutes with the measured instrument response function of the OMA (similar to Fig. 5a), and calibrates the absolute intensity by obtaining pure rotational Raman spectra similar to that of Fig. 5d and using the known differential rotational Raman cross section of

5.4×10^{-30} cm^2/sr for $J = 6 \rightarrow 8$ transition of nitrogen at 488.0 nm (Ref. 24). Note that the differential Thomson scattering cross section is given by[1]

$$\frac{d\sigma}{d\Omega} = \left(\frac{e^2}{4\pi\varepsilon_0 m_e c^2}\right)^2 \sin^2\phi = r_e^2 \sin^2\phi \tag{3}$$

where $r_e = 2.817 \times 10^{-15}$ m is the classical electron radius and ϕ is the angle between the incident laser beam polarization vector and the scattered light propagation direction. From Eq. (3), for vertically polarized scattering ($\phi = 90$ deg), the differential Thomson scattering cross section is equal to 7.94×10^{-26} cm^2/sr. Also note that although the Thomson scattering cross section is independent of wavelength, the rotational Raman cross section has been scaled to 780 nm assuming the well known ν^4 dependence. From this procedure, the inferred values of electron number density and temperature are 3.7×10^{13} cm^{-3} and 0.63 eV, respectively. Corresponding values for the potential electron density and electron temperature that could be measured with the current instrument, based on the statistical uncertainties (2σ) provided by the least-squares fitting procedure,[25] are 8.0×10^{11} cm^{-3} and 0.025 eV. We anticipate future improvements of approximately one order of magnitude in the sensitivity for electron density by a combination of improved optical collection efficiency and increased laser output energy.

Although we have not performed any additional diagnostic measurements on the discharge, we can estimate the electron density by consideration of the measured current–voltage characteristics. From simple continuity, the current density i/A is given by

$$i/A = \rho_e \upsilon_d \tag{4}$$

where ρ_e is the electron density, υ_d is the electron drift velocity, and A is the discharge cross-sectional area. Values of υ_d as a function of E/N, the reduced electric field, can be found by McDaniel.[26] From Fig. 11-3-13 of Ref. 26, and assuming an argon temperature and pressure of 600 K and 3950 Pa, respectively, the drift velocity is found to be $\sim 1.33 \times 104$ m/s at E/N of 4 V $\cdot$ cm^{-1} $\cdot$ torr^{-1} (1.1×10^{-16} V $\cdot$ cm^2). For our estimated discharge diameter of between 1 and 2 mm, Eq. (4) predicts an electron density in the range $1.5 \times 10^{13} - 6 \times 10^{13}$ cm^{-3}, which is reasonably consistent with the measured value of 3.7×10^{13} cm^{-3}.

Evaluation of SBS Phase Conjugate Cell

Despite the significant reduction in stray scattering afforded by the rubidium vapor filter, spectra such as that shown in Fig. 7 are still subject to systematic error due to the small, but finite, nonrejected, residual stray light. For example, the data displayed in Fig. 7 are what result after subtraction of a small mean residual stray light component, the peak magnitude of which was measured to be $\sim$10% of the net peak Thomson signal. At relatively high electron density, such as that measured in Fig. 7, the primary effect of this residual transmitted light is to introduce uncertainty in the inferred value of electron temperature. To assess this, we have altered the mean residual by $\pm$50% and reperformed the least-squares curve fits. As can be seen from Fig. 8, the fits themselves appear to be equally good as that displayed in Fig. 7. Whereas there is virtually no effect on the inferred value of electron density, the values for electron temperature change slightly, by approximately $\pm$0.025 eV, which is essentially the same as the 2σ value for the statistical uncertainty.

At lower values of electron density, where the signal is even weaker than that in Fig. 7, residual stray light is a more significant potential problem. We have performed some preliminary measurements employing the dispersing prisms and SBS cell to assess the potential to further reduce the residual broadband component of the seeded laser. This approach is similar to that described in Ref. 16 except that the pinhole spatial filter in that system has been replaced by the SBS cell. SBS is often employed to filter broadband ASE, which is superimposed upon the narrowband output of dye and/or solid state lasers.[27] Its use, however, is based primarily on the increased divergence of the ASE component, which does not spatially overlap the focused "pump" beam in the SBS cell. (The increased linewidth of the ASE also plays a role, albeit a smaller one.[27]) In a similar manner, the purpose of the prisms in our apparatus is to disperse the broadband unlocked component of the titanium:sapphire laser so that, after focusing into the SBS cell, its spatial overlap with the narrowband pump (and, hence, SBS reflection) will be reduced.

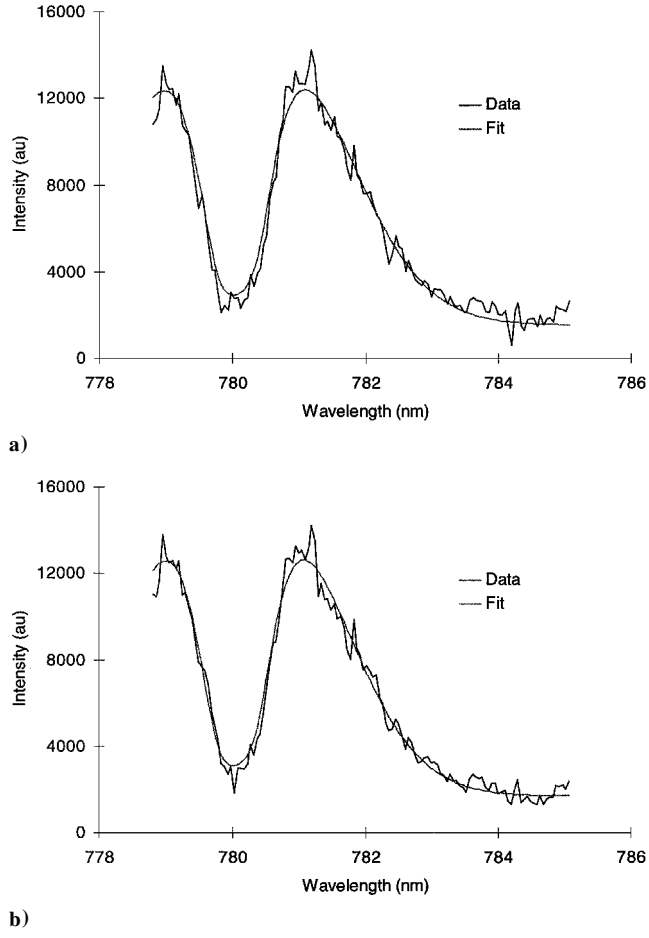

Fig. 8 Least-squares fits to spectrum of Fig. 7 with residual background arbitrarily changed by a) +50%, $Te = 0.65 \pm 0.035$ eV (2σ), and $\rho_e = 3.7 \times 10^{13} \pm 9.3 \times 10^{11}$ cm^{-3} (2σ) and b) −50%, $Te = 0.60 \pm 0.025$ eV (2σ), and $\rho_e = 3.7 \times 10^{13} \pm 8.0 \times 10^{11}$ cm^{-3} (2σ).

Inclusion of the SBS cell with seeding configuration B, while reducing the available laser pulse energy by a factor of approximately four (due to SBS losses), resulted in filter rejection that was sufficiently high that it was difficult to measure directly from rotational Raman spectra. However, some insight can be gained from Fig. 9, which shows the very weak residual transmitted light obtained from an evacuated cell with very long (10-min) integration time. Figures 9a and 9b show the residual scattering without/with, respectfully, incorporation of the SBS cell. As alluded to in the previous section, Fig. 9a shows that the peak residual transmission through the filter is $\sim 6 \times 10^{-6}$. Although it is difficult to see by eye in Fig. 9b, the principal effect of the SBS cell is to reduce the linewidth and, therefore, the integrated intensity, of the residual transmitted light. This can be seen much more clearly in Fig. 10, which is similar to Fig. 9 except that a small additional quantity of stray scattered light from optical elements has purposefully been allowed to "leak" into the spectrometer without being transmitted through the rubidium filter. It can be seen that, when the SBS cell is employed, the residual light is spectrally narrower, with linewidth essentially equal to the 0.20-nm resolution of the spectrometer. We estimate that the effective spectral purity of the entire system, laser and SBS cell, has been further improved to $\sim$0.99998. We plan future measurements to determine this more accurately.

As a further test of the SBS cell, some preliminary Thomson spectra have been obtained. Figure 11 is a representative spectrum, along with least-squares fit, obtained under identical conditions to that of Figs. 6 and 7, except that the dispersing prisms and SBS cell

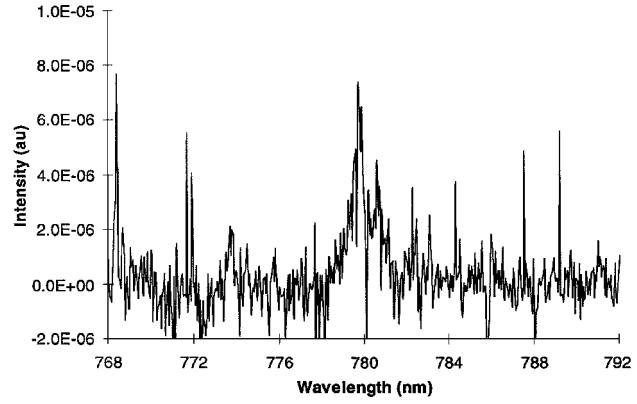

a) Without SBS cell

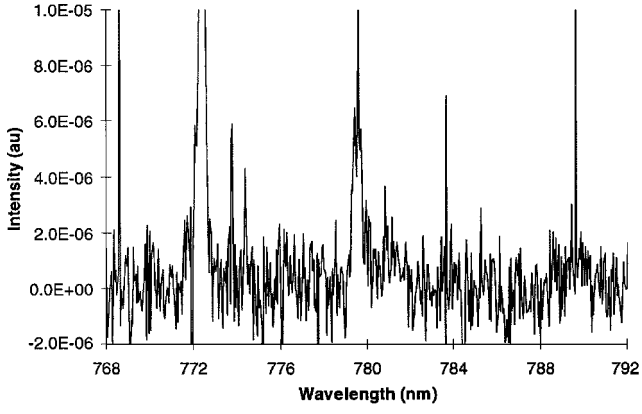

b) With SBS cell

Fig. 9 Residual transmitted scattering from evacuated cell using seeding configuration B.

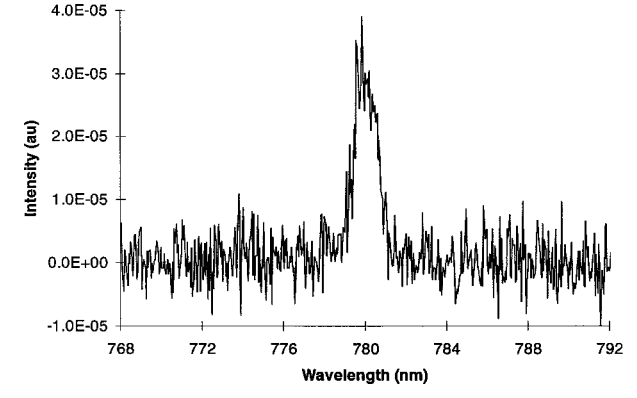

a)

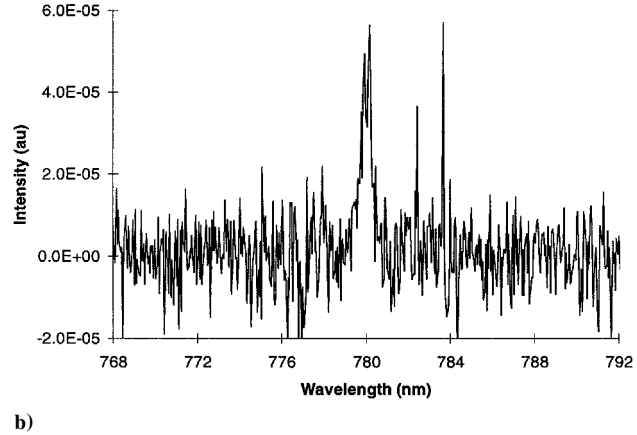

b)

Fig. 10 Similar to Fig. 9 except that stray light has been purposefully allowed to leak into spectrometer to better illustrate linewidth difference between a) without SBS cell and b) with SBS cell.

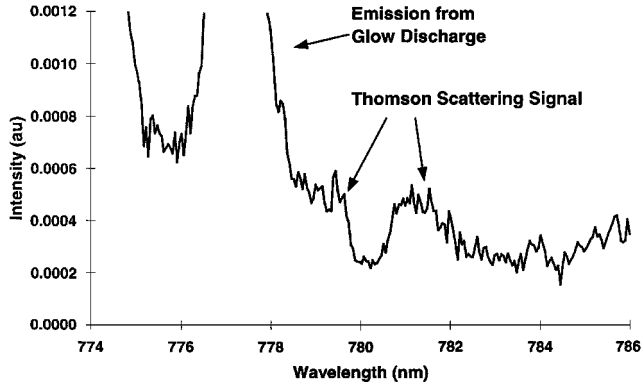

a)

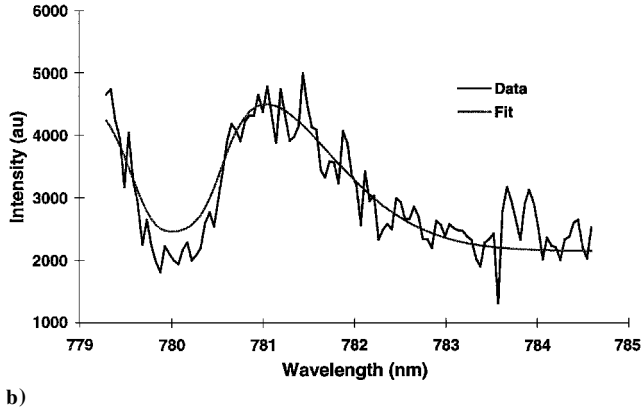

b)

Fig. 11 Thomson scattering spectrum and least-squares fit obtained using dispersing prisms and SBS cell; electron density 1.13×10^{13} cm^{-3} and electron temperature 0.53 eV.

were employed and the electron density was lowered to a value of approximately 1.1×10^{13} cm^{-3}. It can be seen that the signal-to-noise ratio is reduced as a result of the factor of approximately four loss in the incident laser beam intensity (discussed earlier) and the approximate factor of three decrease in electron density. The least-squares fitting procedure returns a value of $1.13 \times 10^{13} \pm 9.0 \times 10^{11}$ (2σ) cm^{-3} and 0.53 ± 0.08 eV (2σ) for the electron number density and temperature, respectively.

It is stressed that sources of residual transmitted background signal are still being explored. In particular, it appears that a significant portion, if not the majority, is from stray light that is scattered from the numerous optical and other surfaces and is "seen" by the detector without following the principal imaging path. We have incorporated baffling and other approaches to minimize this, but it is not yet clear whether its contribution has been completely minimized. Nonetheless, these preliminary results appear to indicate that the incorporation of the prism-SBS cell does reduce the impact of residual stray light, although this is achieved at the cost of reduced signal levels. We plan to evaluate the utility of the SBS cell in more detail in the near future, with emphasis on improving the net reflection efficiency.

Conclusions

A new spectrally filtered light scattering apparatus is presented that incorporates an external cavity diode laser injected seeded titanium:sapphire laser and an optically thick rubidium vapor filter at 780 nm. In a detailed set of measurements, the realizable attenuation of quasi elastically scattered light, which is limited by the existence of a broad spectral linewidth, unseeded component to the laser output, has been determined. It is found that the magnitude of this broadband component is a strong function of the circulating power of the seed laser within the titanium:sapphire laser cavity. Injection of the seed laser through the titanium:sapphire output coupler, employing a Faraday optical isolator, resulted in a measured peak transmission value of approximately 6×10^{-6}, corresponding to a spectral purity of 0.9998. Preliminary measurements indicate that

incorporation of a set of dispersing prisms and an SBS phase conjugate mirror appear to provide an additional factor of 10 extinction.

The utility of the system for measurement of electron density and temperature by Thomson scattering was demonstrated in an argon dc constricted glow discharge. At 100-mA current and 3950 Pa of argon, an electron density of 3.7×10^{13} cm^{-3} was measured on the discharge centerline with a 2σ value of statistical uncertainty equal to 8.0×10^{11} cm^{-3}. The corresponding electron temperature was measured to be 0.63 ± 0.025 eV.

Acknowledgments

The authors acknowledge the sponsorship of the National Science Foundation, Physics Division, and the Director of Defense Research and Engineering within the Air Plasma Ramparts Program managed by the Air Force Office of Scientific Research. The authors would like to acknowledge Glen Rines, of Q-Peak, Inc., for fabrication and installation of the titanium:sapphire breadboard laser.

References

[1]Hutchinson, I. H., *Principles of Plasma Diagnostics*, Cambridge Univ. Press, Cambridge, England, U.K., 1990, pp. 242–258.

[2]Lee, H. G., Lee, S. G., Kim, B. C., Hong, J., Kim, W. C., Choh, K. K., Choi, J. H., Yang, J. G., Na, H. K., Doh, C. J., Hwang, S. M., Kwon, M., and Won, Y. H., "Measurements of the Electron Temperature by the Thomson Scattering System on the Hanbit Magnetic Mirror Device," *Review of Scientific Instruments*, Vol. 72, No. 1, 2001, pp. 1118–1121.

[3]Glenzer, S. H., Divol, L. M., Berger, R. L., Geddes, C., Kirkwood, R. K., Moody, J. D., Williams, E. A., and Young, P. E., "Thomson Scattering Measurements of Saturated Ion Waves in Laser Fusion Plasmas," *Physical Review Letters*, Vol. 86, No. 12, 2001, pp. 2565–2568.

[4]Noguchi, Y., Matsuoka, A., Bowden, M. D., Uchino, K., and Muraoka, K., "Measurements of Electron Temperature and Density of a Micro-Discharge Plasma Using Laser Thomson Scattering," *Japanese Journal of Applied Physics*, Vol. 40, No. 1, 2001, pp. 326–329.

[5]Rasetti, F., "Sopra lo Spettro Raman dell'Ossido Nitrico," *Nuovo Cimento*, Vol. 7, 1930, p. 261–269 (in Italian).

[6]Pelletier, M. J., "Ultraviolet Raman Spectroscopy Using an Atomic Vapor Filter and Incoherent Excitation," *Applied Spectroscopy*, Vol. 46, No. 3, 1992, pp. 395–400.

[7]Indralingan, R., Simeonsson, J. B., Petrucci, G. A., Smith, B. W., and Winefordner, J. D. W., "Raman Spectrometry with Metal Vapor Filters," *Analytical Chemistry*, Vol. 64, 1991, pp. 964–967.

[8]Clops, R., Fink, M., Varghese, P. L., and Young, D., "Thermodynamic Studies of Subsonic Gas Flow Using a Laser Diode Raman Spectrometer," *Applied Spectroscopy*, Vol. 54, No. 9, 2000, pp. 1391–1398.

[9]Shimizu, H., Lee, S. A., and She, C. Y., "High Spectral Resolution Lidar System with Atomic Blocking Filters for Measuring Atmospheric Parameters," *Applied Optics*, Vol. 22, No. 9, 1983, pp. 1373–1381.

[10]Miles, R. B., Yalin, A. P., Tang, Z., Zaidi, S. H., and Forkey, J. N., "Flow Field Imaging Through Sharp-Edged Atomic and Molecular 'Notch' Filters," *Measurement Science and Technology*, Vol. 12, No. 4, 2001, pp. 442–451.

[11]Elliott, G. S., Glumac, N., and Carter, C. D., "Molecular Filtered Rayleigh Scattering Applied to Combustion," *Measurement Science and Technology*, Vol. 12, No. 4, 2001, pp. 452–466.

[12]Hoffman, D., Munch, K.-U., and Leipertz, A., "Two-Dimensional Temperature Determination in Sooting Flames by Filtered Rayleigh Scattering," *Optics Letters*, Vol. 21, No. 7, 1996, pp. 525–527.

[13]Rines, G. A., and Moulton, P. F., "Performance of Gain-Switched Ti:Al_2O_3 Unstable-Resonator Lasers," *Optics Letters*, Vol. 15, No. 8, 1990, pp. 434–436.

[14]Finkelstein, N. D., Lempert, W. R., Miles, R. B., Finch, A., and Rines, G. A., "Cavity Locked, Injection Seeded, Titanium:Sapphire Laser and Application to Ultraviolet Flow Diagnostics," AIAA Paper 96-0177, Jan. 1996.

[15]Zaidi, S., Tang, Z., Yalin, A., Barker, P., and Miles, R., "Filtered Thomson Scattering in an Argon Plasma," AIAA Paper 2001-0415, Jan. 2001.

[16]Bakker, L. P., Freriks, J. M., deGroog, F. J., and Kroesen, G. M. W., "Thomson Scattering Using an Atomic Notch Filter," *Review of Scientific Instruments*, Vol. 71, No. 5, 2000, pp. 2007–2014.

[17]Ni, C. K., and Kung, A. H., "Effective Suppression of Amplified Spontaneous Emission by Stimulated Brillouin Scattering Phase Conjugation," *Optics Letters*, Vol. 21, No. 20, 1996, pp. 1673–1675.

[18]Lee, W., Adamovich, I. V., and Lempert, W. R., "Optical Pumping Studies of Vibrational Energy Transfer in High-Pressure Diatomic Gases," *Journal of Chemical Physics*, Vol. 114, No. 3, 2001, pp. 1178–1186.

[19]Gustafsson, J., Rojas, D., and Axner, O., "The Influence of Hyperfine Structure and Isotope Shift on the Detection of Rb Atoms in Atmospheric Pressure Atomizers by the 2f-Wavelength Modulation Technique," *Spectrochimica Acta, Part B: Atomic Spectroscopy*, Vol. 52, No. 13, 1997, pp. 1937–1953.

[20]Barwood, G. P., Gill, P., and Rowley, W. R., "Frequency Measurements on Optically Narrowed Rb-Stabilised Laser Diodes at 780 nm and 795 nm," *Applied Physics B*, Vol. 53, No. 3, 1991, pp. 142–147.

[21]Yalin, A. P., Barker, P. F., and Miles, R. B., "Characterization of Laser Seeding by Use of Group-Velocity Dispersion in an Atomic-Vapor Filter," *Optics Letters*, Vol. 25, No. 7, 2000, pp. 502–504.

[22]Barnes, J. C., Barnes, N. P., Wang, L. G., and Edwards, W., "Injection Seeding I: Theory," *IEEE Journal of Quantum Electronics*, Vol. 29, No. 10, 1993, pp. 2670–2683.

[23]Barnes, J. C., Barnes, N. P., Wang, L. G., and Edwards, W., "Injection Seeding II: Ti:Al_2O_3 Experiments," *IEEE Journal of Quantum Electronics*, Vol. 29, No. 10, 1993, pp. 2684–2692.

[24]Penney, C. M., St. Peters, R. L., and Lapp, M., "Absolute Rotational Raman Cross Sections for N_2, O_2 and CO_2," *Journal of the Optical Society of America*, Vol. 64, No. 5, 1974, pp. 712–716.

[25]Bevington, P. R., *Data Reduction and Error Analysis for the Physical Sciences*, McGraw–Hill, New York, 1969, pp. 141–161.

[26]McDaniel, E. W., *Collisional Phenomena in Ionized Gases*, Wiley, New York, 1964, pp. 592–653.

[27]Ni, C. K., and Kung, A. H., "Amplified Spontaneous Emission Reduction by Use of Stimulated Brillouin Scattering: 2-ns Pulses from Ti:Al_2O_3 Amplifier Chain," *Applied Optics*, Vol. 37, No. 3, 1998, pp. 530–535.

R. P. Lucht
Associate Editor